

# **PV System Based MPPT Controller Supplying BLDC Motor Drive**

S.Selvakani<sup>1</sup>, D.Sindhu<sup>2</sup>, R.Anand<sup>3</sup>

PG Scholar, Department of EEE, Sri Krishna College of Technology, Coimbatore, India<sup>1</sup>

PG Scholar, Department of EEE, Sri Krishna College of Technology, Coimbatore, India<sup>2</sup>

Assistant Professor, Department of EEE, Sri Krishna College of Technology, Coimbatore, India<sup>3</sup>

**ABSTRACT:** This paper presents photovoltaic system with a maximum power point tracking (MPPT) controller is connected to brushless dc motor drive for heating, ventilating and air conditioning fans. The MPPT controller is based on a genetic assisted, multi-layer perceptron neural network (GA-MLP-NN) structure and includes a DC-DC boost converter. Genetic assistance in the neural network is used to optimize the size of the hidden layer. Also, for training the network, a genetic assisted, Levenberg-Marquardt (GA-LM) algorithm is utilized. The off line GA-MLP-NN, trained by this hybrid algorithm, is utilized for online estimation of the volt-age and current values in the maximum power point. A brushless dc (BLDC) motor drive system that incorporates a motor controller with proportional integral (PI) speed control loop is successfully implemented to operate the fans. The digital signal processor (DSP) based unit provides rapid achievement of the MPPT and current control of the BLDC motor drive.

**KEYWORDS:** Photovoltaics; MPPT; DSP; Artificial neural networks; Genetic algorithms; Brushless dc motors

## **1. INTRODUCTION**

The photovoltaic (PV) energy make it one of the most promising energy alternatives. Since PV electricity is expensive compared to electricity from the utility grid, stand alone applications of PV energy are more favorable. They are particularly utilized for applications like powering residential appliances, electrification of villages in rural areas, telecommunications, heating, ventilating and air conditioning (HVAC) applications, water pumping etc. Although HVAC applications and PV energy show a complementary nature as the trends of supply and demand loads match with time of the day, there is not enough literature about HVAC applications of PV energy. Also, it seems that not enough attention has been given to PV systems feeding brushless DC (BLDC) motor loads, despite these motors' favorable features such as high reliability, high efficiency, less maintenance requirements and reduced environmental effects. In various contributions, brushed DC motor or induction motor loads are considered. The performance of DC motors supplied from PV sources has been analyzed by Appelbaum[1]. Two low cost PV utilization schemes for ventilation and air conditioning loads have been presented in Ref. [2]. In that study, permanent magnet DC (PMDC) type and AC induction type motors have been employed. Vector control of an induction motor fed by a PV generator is presented in Ref. [3]. Our work demonstrates that compared with other studies in the field, the use of a BLDC motor, which exhibits the highest efficiency among all conventional motors, provides an effective demand side energy management technique.

Because the energy conversion efficiency of PV generators is low, a proper matching between the PV generators and the electric load should be considered. Therefore, the coupling between the motor load and the PV module is implemented via a maximum power point tracking (MPPT) controller to operate the PV system at its maximum output power for any temperature and solar radiation level. Various MPPT methods have been considered in PV power applications. Among the hill climbing methods [4-6], the perturb and observe (P&O) method tracks the maximum power point (MPP) by repeatedly increasing or decreasing the output voltage at the MPP of the PV module. The implementation of the method is relatively simple, but it cannot track the MPP when the irradiance varies quickly with time. In addition, it may cause system oscillation around the peak power points due to the effect of measurement noise. The incremental conductance method is also often used in PV systems [7,8]. This method tracks the MPPs by

# International Journal of Innovative Research in Science, Engineering and Technology

(An ISO 3297: 2007 Certified Organization)

Vol. 4, Special Issue 6, May 2015

comparing the incremental and instantaneous conductance's of the solar array. This method requires more conversion time, and a large amount of power loss results. In addition, extra hardware circuitry is required to implement the system. Neural network (NN) based MPPT techniques have been proposed [9–11]. Compared to the conventional methods, these studies show that this modern control algorithm is capable of improving the tracking performance. The method requires little or no knowledge of the PV parameters, and the trained NN can provide a sufficiently accurate MPPT. A PC based MPP tracker for a PV system using NNs has been developed by Ref. [9]. The system consisted of a PV module with a MPP tracker and a DC motor driving an air fan. Solar array modeling and MPP tracking is studied in Ref. [10], and two NNs, which are back propagation NN and radial basis function NN, are compared. It is shown that the back propagation NN needed less information for training. The use of radial basis function networks (RBFN) for solar array modeling and MPP prediction is presented in Ref. [11]. It shows that an RBFN model can be trained faster than a multi-layer perceptron (MLP) model. However, the DSP implementation of this network is more difficult. In our study, the proposed MPPT technique utilizes the genetic assisted, multi-layer perceptron neural network (GA-MLP-NN) trained by the genetic assisted, Levenberg–Marquardt (GA-LM) method.

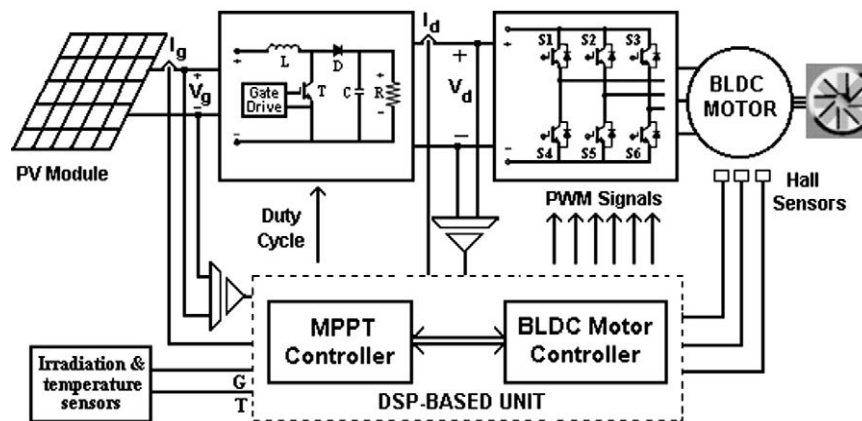


Fig. 1. The diagram of the implemented system

The use of genetic assistance helps in optimizing the size of the hidden layer of the NN. By adopting an evolutionary algorithm, implementing such a hybrid system helps use the advantages of both the Levenberg–Marquardt (LM) algorithm, which is a higher order adaptive algorithm for minimizing the mean square error (MSE) of a NN, and the robustness, speed, efficiency and flexibility features of genetic algorithms (GA). Since our neural network implementation is run in a recall mode, the complexity of the training algorithm and the disadvantage of slow training cause no difficulties.

This study aims to show that employing an effective MPPT controller and replacing a conventional motor like the brushed DC or induction motor with a BLDC motor can accomplish a considerable energy saving in a standalone PV power system operating HVAC fans. The overall diagram of the implemented system is shown in Fig. 1. Solar insolation is converted to DC electrical power, and the MPPT controller output supplies the BLDC motor drive to operate the fans. In the MPPT controller, the GA-MLP-NN is used, and the system robustness and insensitivity to intermittent weather conditions is enhanced. The BLDC motor controller is used to decode position data coming from the Hall effect sensors and generates switching signals for the three phase power stage to electronically commutate the motor. The speed controller also implements a simple proportional integral (PI) control loop. The power stage combines a three phase inverter circuit. The implementation of the overall system is based on a DSP unit. The matching of the supply and demand loads with time of the day makes the system widely applicable.

## II. PV ARRAY CHARACTERISTICS

The basic element of a PV system is the solar cell. A typical solar cell consists of a p–n junction formed in a semiconductor material similar to a diode. As shown in Fig. 2, the equivalent circuit model of a solar cell consists of a

## International Journal of Innovative Research in Science, Engineering and Technology

(An ISO 3297: 2007 Certified Organization)

Vol. 4, Special Issue 6, May 2015

current generator ( $I_L$ ) and a diode plus series ( $R_s$ ) and parallel resistances ( $R_{sh}$ ) [12].

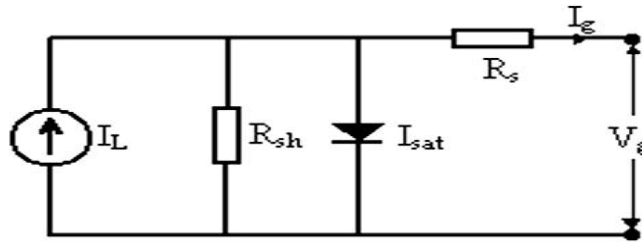


Fig. 2. The equivalent circuit of a solar cell

The current–voltage characteristic of a single cell when neglecting the internal shunt resistance is described by the Shockley solar cell equation [13]:

$$I_g = I_L - I_{sat} \left( \exp\left(\frac{QV_{oc}}{AKT}\right) - 1 \right)$$

where  $I_g$  is the output current,  $I_L$  is the generated current under a given insolation,  $I_{sat}$  is the diode saturation current,  $V_{oc}$  is the open circuit voltage,  $K$  is Boltzmann's constant,  $Q$  is the electron charge,  $T$  is the temperature (K) and  $A$  is the ideality factor for a p–n junction. The saturation current ( $I_{sat}$ ) of the solar array varies with temperature according to the following equation:

$$I_{sat} = I_r \left[ \frac{T}{T_r} \right]^3 \left[ \exp\left[ \frac{QE_{GO}}{KA} \right] \left( \frac{1}{T_r} - \frac{1}{T} \right) \right]$$

where  $T_r$  is the reference temperature,  $I_r$  is the saturation current at  $T_r$ ,  $T$  is the temperature of the solar array (K) and  $E_{GO}$  is the band gap energy of the semiconductor used in the solar array.  $I_L$  in Eq. (1) is a function of incident solar radiation and cell temperature and is given as

$$I_L = [I_{scr} + K_I(T - 25)] \frac{S}{100}$$

where  $I_{scr}$  is short circuit current at  $T_r$ ,  $K_I$  is the short circuit current temperature coefficient and  $S$  is the insolation in  $mW/cm^2$ . Eqs.(1)–(3) can be applied to simulate the characteristics of solar cells. It is seen that the output characteristics of the solar.

In order to maximize the output power from a array is nonlinear and vitally affected by the solar radiation, temperature and load conditions solar module, it has to be operated at a unique point with specified voltage and current values, or in other words, at a specified load resistance. This requires a separate power converter circuit for the MPPT. In our design, a boost type DC–DC converter is employed to match the load to the PV array to extract the maximum power.

### III. BOOST TYPE DC-DC CONVERTER

In Fig. 3(a), the schematic of the boost converter power stage is given. It consists of the power switch  $T$ , boost inductor  $L$ , filter capacitor  $C$ , output diode  $D$  and load resistor  $R$ . Here, the DC input source voltage  $V_g$  is supplied by the PV modules. The converter steady state waveforms in the continuous conduction mode (CCM) where the inductor current flows continuously ( $i_L > 0$ ) are presented in Fig. 3(b).

When the switch  $T$  is in the on state, the current in the boost inductor increases linearly, and at that time, the diode is in the off state. When the switch  $T$  is turned off, the energy stored in the inductor is released through the diode to the output  $RC$  circuit. The pulsating current produced by the switching action is smoothed by the capacitive filter and a DC voltage is provided to the load. The boost converter transfer function is obtained by considering its steady state operation [14]. The DC voltage transfer function is

$$\frac{V_d}{V_g} = \frac{1}{1 - D}$$

## International Journal of Innovative Research in Science, Engineering and Technology

(An ISO 3297: 2007 Certified Organization)

Vol. 4, Special Issue 6, May 2015

Assuming a lossless circuit,  $P_g = P_d$

$$V_d I_d = V_g I_g \Rightarrow \frac{I_d}{I_g} = (1 - D)$$

where  $V_g$  and  $I_g$  is converter input voltage and current (the output voltage and current of the PV array), respectively,  $V_d$  and  $I_d$  is the output voltage and current, respectively,

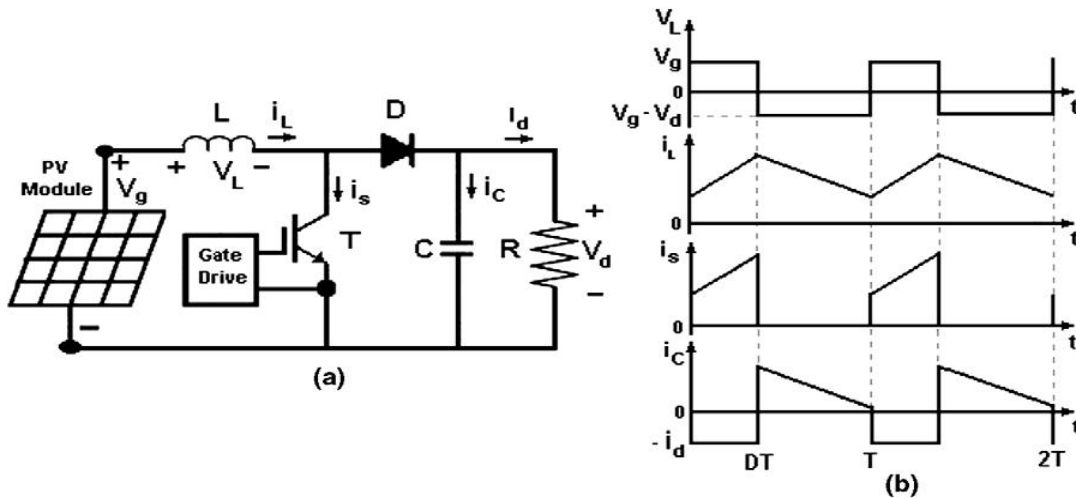


Fig. 3. Boost converter: (a) power stage schematic; (b) waveforms

and  $D$  is the duty ratio of the controllable switch. The boost converter operates in the CCM for  $L > L_{min}$  where

$$L_{min} = \frac{(1 - D)^2 DR}{2f}$$

Here,  $f$  is the switching frequency and  $R$  is the load resistance. The minimum value of the filter capacitance that results in voltage ripple  $V_r$  is given by

$$C_{min} = \frac{V_d D}{V_r R f}$$

As the name of the converter suggests, the output voltage is always greater than the input voltage. Therefore, in our design, the boost converter is used to increase the voltage magnitude for the BLDC motor drive bus voltage and to control the MPPT. The control signal of the converter is obtained from the GA-MLP-NN based MPPT controller, of which the neural network structure and training algorithm is explained in the following section.

### IV. GA-MLP-NN STRUCTURE OF MPPT CONTROLLER

An artificial neural network (ANN) is a massively parallel distributed processor that has a natural tendency for storing experimental knowledge and making it available for use [15]. The power of ANNs in system identification and development of adaptive controllers makes them well suited to PV energy applications such as identification of the optimal operating point of PV arrays. In engineering applications, a multi-layer perceptron network trained by the back propagation (MLP-BP) method is the most widely utilized technique. In MLPs, the units are structured into ordered layers, and connections are allowed only between adjacent layers in an input to output sense. Back propagation (BP) training is a complex gradient descent algorithm. It tries to improve the performance of the NN by reducing the total error by changing the weights along its gradient [16]. Standard gradient descent algorithms use only the local

# International Journal of Innovative Research in Science, Engineering and Technology

(An ISO 3297: 2007 Certified Organization)

Vol. 4, Special Issue 6, May 2015

approximation of the slope of the performance surface (error versus weights) to determine the best direction to move the weights in order to lower the error.

The Levenberg–Marquardt (LM) method is one of the most appropriate higher order adaptive algorithms known for minimizing the MSE, which is one of the most widely used error norms in a NN. The LM algorithm is an approximation to the Newton method used also for training ANNs. The Newton method approximates the error of the network with a second order expression, which contrasts to the BP algorithm that does it with a first order expression. The weight update equations of the LM algorithm are provided in Ref. [17]. The outputs offer very good results compared to other systems utilizing MLP networks trained by the standard gradient descent algorithms.

GAs have been increasingly applied in ANN design in several ways, namely topology optimization, genetic training algorithms and control parameter optimization. In ANN topology optimization, GAs are used to select a topology (number of hidden layers, number of hidden nodes, interconnection pattern) for the ANN, which, in turn, is trained using some training scheme [18]. The GA combines selection, crossover and mutation operators with the goal of finding the best solution to a problem by searching until the specified criterion is met. The solution to a problem is called a chromosome, which is composed of a collection of genes. In hybrid neuro-genetic applications, genes are the NN parameters to be optimized. The GA creates an initial population and then evaluates this population by training a NN for each chromosome. It then evolves the population through multiple generations in the search for the best network parameters. In our study, genetic assistance is used to optimize the number of hidden neurons. Also, a hybrid genetic assisted LM algorithm is accomplished to train the MLP-NN. Thus, it reduces the chance of converging to local minima in which other algorithms might get trapped, and the global optimum of the problem can be approached with higher probability. This training algorithm was compared with separately implemented standard BP algorithm with delta bar delta (BP-DBD) and LM algorithms.

The configuration of the implemented NN to predict the MPPs of the PV array is shown in Fig. 4. The network has three layers, i.e. an input, a hidden and an output layer. The input layer has two nodes for the irradiation and the temperature. The number of nodes in the hidden layer has been determined by genetic assistance. The best result has been obtained for 8 nodes. The output layer has two nodes, and the voltage ( $V_{mp}$ ) and current ( $I_{mp}$ ) at the MPP are the outputs of the NN. In this feed forward NN consisting of a single hidden layer, all the layers of the NN have a hyperbolic tangent transfer function.

## V. BLDC MOTOR DRIVES

A BLDC motor is a rotating electric machine where the stator is a classic three phase stator like that of an induction motor and the rotor has surface mounted permanent magnets. In this respect, the BLDC motor is equivalent to a reversed DC commutator motor in which the magnet

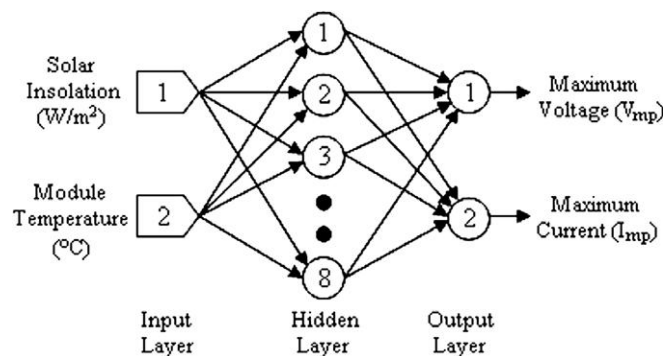


Fig. 4. Boost converter power stage schematic

# International Journal of Innovative Research in Science, Engineering and Technology

(An ISO 3297: 2007 Certified Organization)

Vol. 4, Special Issue 6, May 2015

rotates while the conductors remain stationary. In the DC commutator motor, the current polarity is altered by the commutator and brushes. On the contrary, in the BLDC motor, the polarity reversal is performed by power transistors switching in synchronization with the rotor position. Therefore, BLDC motors often incorporate either internal or external position sensors to sense the actual rotor position [19].

BLDC motor drives require variable frequency, variable amplitude excitation that is usually provided by a three phase, full bridge inverter as shown in Fig. 5(a). The inverter is usually responsible for both the electronic commutation and current regulation [20]. In Fig. 5(b), the back EMF and phase current waveforms for the three phase BLDC motor with 120L bipolar current are shown [20].

The pulse width modulated (PWM) inverter topology has a six switch voltage source configuration with constant dc link voltage ( $V_d$ ), which is identical with induction motor drives and permanent magnet AC motor drives. The analysis is based on the following assumptions for simplification [21]:

Under the above assumptions, a BLDC motor can be represented as [20]

$$\begin{bmatrix} V_a \\ V_b \\ V_c \end{bmatrix} = \begin{bmatrix} R & 0 & 0 \\ 0 & R & 0 \\ 0 & 0 & R \end{bmatrix} \begin{bmatrix} i_a \\ i_b \\ i_c \end{bmatrix} + \begin{bmatrix} L-M & 0 & 0 \\ 0 & L-M & 0 \\ 0 & 0 & L-M \end{bmatrix} \frac{d}{dt} \begin{bmatrix} i_a \\ i_b \\ i_c \end{bmatrix} + \begin{bmatrix} e_a \\ e_b \\ e_c \end{bmatrix}$$

where  $v_a, v_b, v_c$  are the phase voltages,  $i_a, i_b, i_c$  are the phase currents,  $e_a, e_b, e_c$  are the phase back EMF waveforms,  $R$  is the phase resistance,  $L$  is the self inductance of each phase and  $M$  is the mutual inductance between any two phases.

The electromagnetic torque is given by

$$T_e = (e_a i_a + e_b i_b + e_c i_c) / \omega_r$$

where  $\omega_r$  is the mechanical speed of the rotor. The equation of motion is

$$J \frac{d}{dt} \omega_r = (T_e - T_L - B \omega_r)$$

where  $T_L$  is the load torque,  $B$  is the damping constant and  $J$  is the moment of inertia of the drive. The electrical frequency is related to the mechanical speed by

$$\omega_e = \left(\frac{P}{2}\right) \omega_r$$

where  $P$  is the number of motor poles.

Fig. 6 describes the basic building blocks of the BLDC motor drive. The drive system consists of the PI speed controller, reference current generator, PWM current controller, Hall-IC position sensor, 3 phase inverter and the

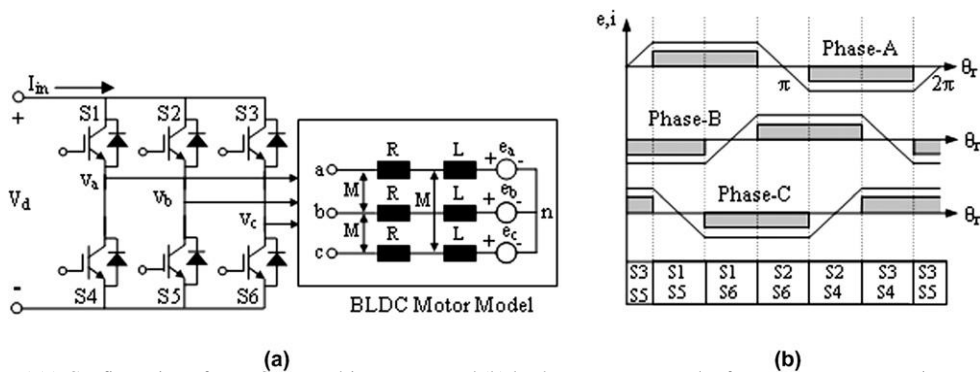


Fig. 5.(a) Configuration of BLDC motor drive system and (b) back EMF pattern and reference current generation.

# International Journal of Innovative Research in Science, Engineering and Technology

(An ISO 3297: 2007 Certified Organization)

Vol. 4, Special Issue 6, May 2015

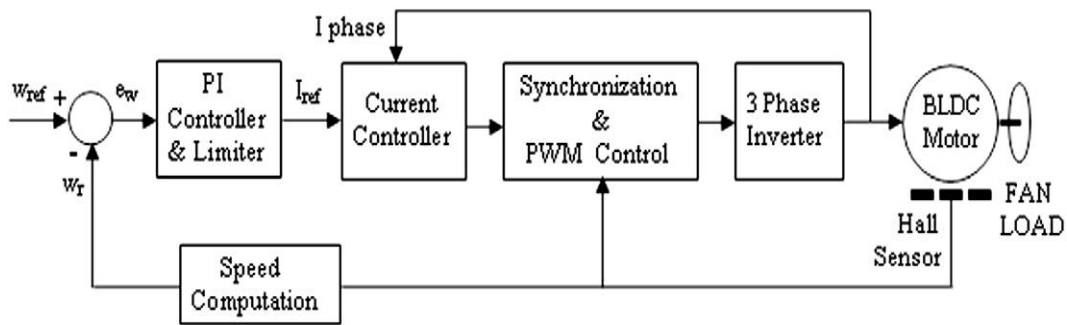


Fig. 6. Block diagram of BLDC motor drive

motor-load union. The speed of the motor is compared with its reference value, and the speed error is processed in the PI speed controller. The output of this controller is considered as the reference torque. A limit is put on the speed controller output depending on the permissible maximum winding currents. The reference current generator block generates the three phase reference currents using the limited peak current magnitude decided by the controller and the position sensor. The PWM current controller regulates the winding currents ( $i_a, i_b, i_c$ ) within the small band around the reference currents. The motor currents are compared with the reference currents, and switching commands are generated to drive the inverter devices [22].

Because of its simple structure and easy implementation, the PI controller is widely used in industrial control systems. A speed error signal ( $e$ ) is input to the PI controller, and in the digital control system, an error expression for the  $n$ th sample is determined by the following:

$$e(n) = w_{ref}(n) - w_r(n)$$

The PI controller output value in terms of torque is given by

$$T(n) = T(n - 1) + K_p(e(n) - e(n - 1)) + K_i\{e(n)\}$$

where  $e(n)$  is the current error signal,  $e(n - 1)$  is the previous error value,  $K_p$  is the proportional gain and  $K_i$  is the integral gain. These constants are dependent on the process and are determined in compliance with the desired starting and continuous time responses.

## VI. SIMULATION AND EXPERIMENTAL RESULT

The prototype system has been developed using the above explained method and tested in the laboratory. The overall system is controlled by an ADSP-21992 Digital Signal Processor. The DSP unit has a 160 MHz, ADSP-219x DSP core and features an 8-Channel, 14-Bit, 20 MSPS ADC with On-Chip voltage reference. Also, it features a three phase PWM generation unit with additional auxiliary PWM outputs and three 32 bit general purpose timers. With the DSP based unit, the GA-MLP-NN based MPP tracking and current control of the BLDC motor drive can be achieved rapidly. Two parallel connected PV modules with a total maximum power of 120 W have been used in the system. The specification of the PV modules provided by the manufacturer is given in Table 1.

# International Journal of Innovative Research in Science, Engineering and Technology

(An ISO 3297: 2007 Certified Organization)

Vol. 4, Special Issue 6, May 2015

Table 1  
Specification of PV module at STC (25 LC and 1 kW/m<sup>2</sup>)

Parameters	Value
Maximum power, $P_{max}$	60 W
Nominal current, $I_{MPP}$	3.55 A
Nominal voltage, $V_{MPP}$	16.9 V
Short circuit current, $I_{SC}$	3.73 A
Open circuit voltage, $V_{OC}$	21.5 V

Table 2  
Parameters of BLDC motor

Parameters	Value	Dimension
R	0.348	X
L	0.314	MH
$K_e$	0.0419	V/(rad/s)
J	$19 \cdot 10^{-6}$	kg m <sup>2</sup>
B	0.000	N m/s
$K_t$	0.0419	kg m/A

For solar radiation and temperature measurements, a silicon irradiance sensor has been used. The sensor has active temperature compensation, and its irradiance measurement error with temperature compensation is  $\pm 6\%$ , and the temperature measurement accuracy at 25 LC is  $\pm 1.5$  LC. The power switch of the boost converter is an IGBT device rated at 200 V, 12 A, and the fast recovery diode has 200 ns reverse recovery time. The calculated out-put capacitor value is 470  $\mu$ F, and the boost inductor value is 350  $\mu$ H. The BLDC motor, which is coupled to the ventilating fan, is a 24 V, 106 W, 8 pole BLDC motor. The parameters of the BLDC motor are given in Table 2.

This NN topology has been trained for three different training algorithms to obtain the accuracies of each method. The algorithms used are BP training using the delta bar delta (DBD) method, LM algorithm and genetic assisted LM algorithm. The network is pre-trained by using 400 data points randomly generated by Eqs. (1)–(3). The number of training iterations is 10,000; the error goal is  $1 \cdot 10^{-10}$ ; and the activation function of the neurons is the tangent hyperbolic function. The weight and bias values obtained from off line training of these three methods are used to validate the MPPT controller operation. In Table 3, it is seen that comparing with other conventional methods, GA-LM training offers the best results.

For testing the MPP tracking, another group of 70 random input–output data points were used. The error of the maximum current and maximum voltage for the three methods are calculated and compared with the information from the mathematical model as shown in Table 4. The superiority of the estimation of the proposed GA-LM hybrid algorithm is seen in Table 4.

## International Journal of Innovative Research in Science, Engineering and Technology

(An ISO 3297: 2007 Certified Organization)

Vol. 4, Special Issue 6, May 2015

measured maximum power (MP), the maximum power pre-dicted by the GA-MLP-NN based MPPT (MPGA) and the normal operating power (NOP) (power delivered by PV module when it is directly coupled to the load without the MPPT). These values have been obtained for every 15 minutes throughout the given day with a solar module orientation of 33L. It shows that NOP is much less than the power taken by the load in the case of using the MPPT controller and an average of 25–35% power increase is gained by the proposed MPPT controller.

The laboratory implemented system has been tested, and waveforms have been obtained to show the performance of the system. Figs. 8 and 9 present the variations of instanta- Fig. 8. PV module output voltage and current waveforms (voltage: 5 V/ div, current: 5 A/div, time: 1 s/div).

PV module output voltage and current waveforms and boost converter output voltage and current wave-forms, respectively, for a step change of insolation (from 700 W/m<sup>2</sup> to 900 W/m<sup>2</sup> at 45 LC).

Fig. 10 shows the phase to phase voltage and phase cur-rent waveforms of the BLDC motor obtained when it is coupled to an air fan and loaded from the MPPT control-ler. Fig. 11 shows the variation of rotor speed of the BLDC motor for step changes of insolation.

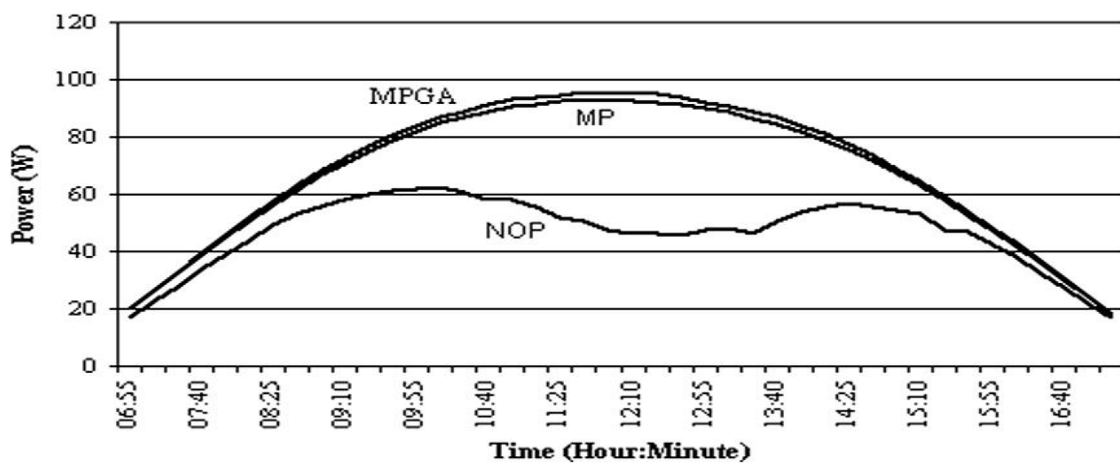


Fig 7.Performance of the pv system

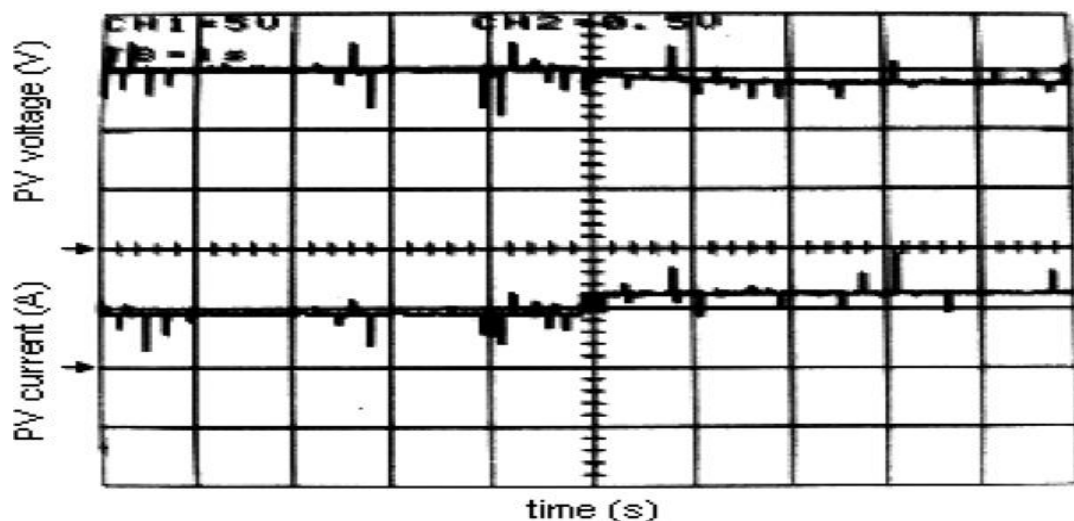


Fig 8.PV module output voltage and current waveforms (voltage: 5 V/ div, current: 5 A/div, time: 1 s/div).

## International Journal of Innovative Research in Science, Engineering and Technology

(An ISO 3297: 2007 Certified Organization)

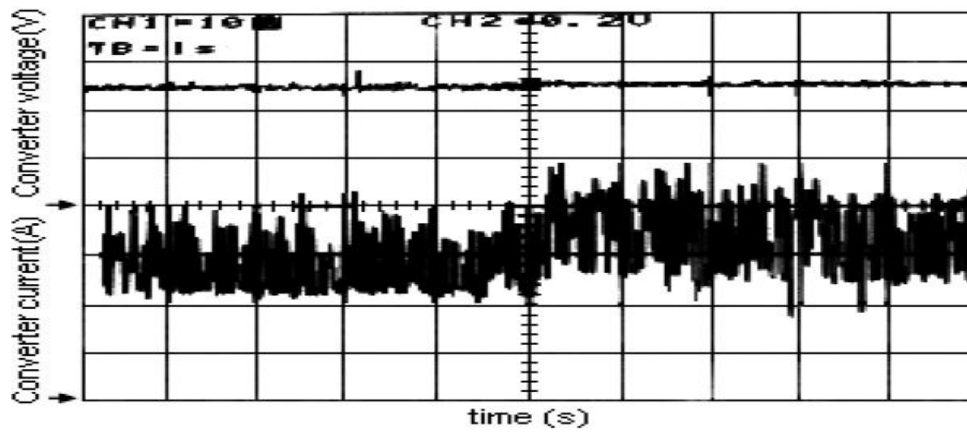


Fig. 9. Boost converter output voltage and current waveforms (voltage: 10 V/div, current: 1 A/div, time: 1 s/div).

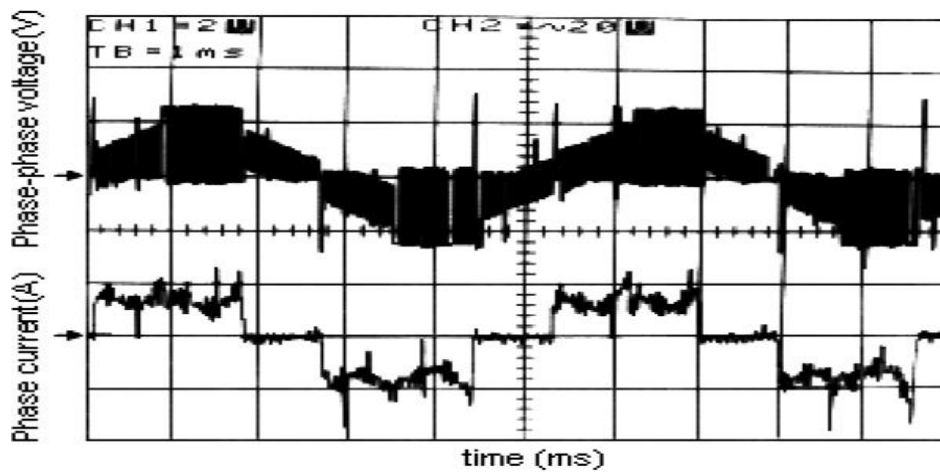


Fig. 10. Phase to phase voltage and phase current waveforms of the BLDC motor (voltage: 20 V/div, current: 2 A/div, time: 1 ms/div).

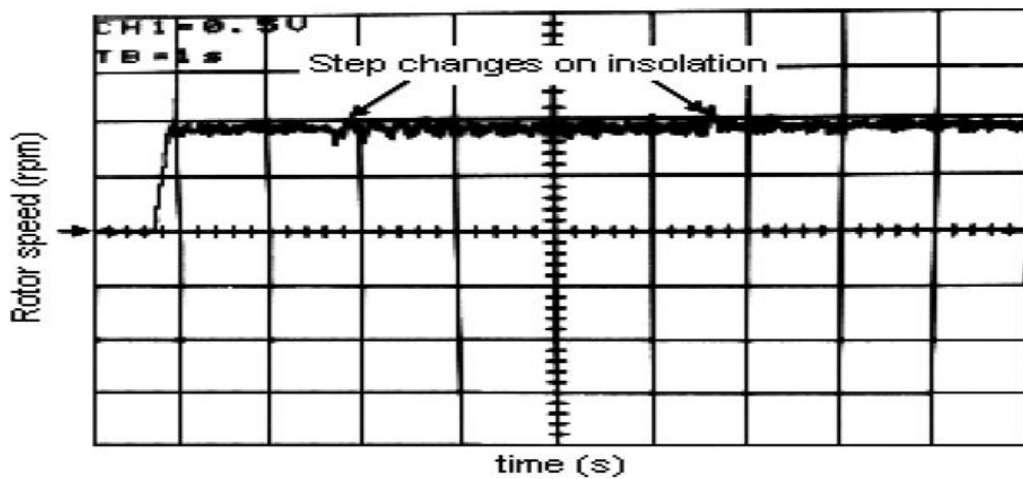


Fig. 11. Variation of rotor speed of BLDC motor for step changes on insolation (speed: 1500 rpm/div, time: 1 s/div).

# International Journal of Innovative Research in Science, Engineering and Technology

(An ISO 3297: 2007 Certified Organization)

Vol. 4, Special Issue 6, May 2015

## VII. CONCLUSION

PV system with a GA-MLP-NN based MPPT controller and 3 phase BLDC motor drive has been designed and tested. From the results acquired in a day with high radiation levels, it is seen that the proposed MPPT controller provides an average power increase of 25.35%. Also, the system could be operated longer periods of time through the day by means of the MPPT controller. The use of genetic assistance provided optimization of the size of the hidden layer. Also, training the NN with the GA-LM algorithm presented better results compared with other systems trained by standard gradient descent algorithms by reducing the chance of converging to local minima. The presented BLDC drive system has been successfully applied to a fan application, and from the experimental results, it has been shown that the use of PI controlled PWM inverter drive can smoothly control the BLDC motor. From the results, it can be concluded that the proposed system can provide an effective energy management technique in PV systems implemented in remote areas.

## REFERENCES

- [1] Appelbaum J. Starting and steady-state characteristics of DC motors powered by solar cell generators. IEEE Trans Energy Convers 1986;1:17–24.
- [2] Sharaf AM, AboulNaga MM, El Diasty R. Building-integrated solar photovoltaic systems – a hybrid solar cooled ventilation technique for hot climate applications. Renew Energy 2000;19:91–6.
- [3] Arrouf M, Bouguechal N. Vector control of an induction motor fed by a photovoltaic generator. Appl Energy 2003;74:159–67.
- [4] Koutroulis E, Kalaitzakis K, Voulgaris NC. Development of a microcontroller-based photovoltaic maximum power point tracking control system. IEEE Trans Power Electron 2001;16(1):46–54.
- [5] Kim Y, Jo H, Kim D. A new peak power tracker for cost-effective photovoltaic power systems. IEEE Proc Energy Convers EngConf IECEC 1996;3(1):1673–8.
- [6] Kuo YC, Liang TJ, Chen JF. Novel maximum power point tracking controller for photovoltaic energy conversion system. IEEE Trans Ind Electron 2001;48(3):594–601.
- [7] Sullivan CR, Powers MJ. A high-efficiency maximum power point tracker for photovoltaic array in a solar-powered race vehicle. Proc IEEE PESC 1993:574–80.
- [8] Hussein KH et al. Maximum photovoltaic power tracking: An algorithm for rapidly changing atmospheric conditions. ProcInst Elect Eng 1995;142(1):59–64.
- [9] Bahgat ABG, Helwa NH, Ahmad GE, El Shenawy ET. Maximum power point tracking controller for PV systems using neural networks. Renew Energy 2005;30:1257–68.
- [10] Premrudeepreechacham S, Patanapirom N. Solar-array modelling and maximum power point tracking using neural networks. In: Power Tech Conference